

2012

# XMM-Newton Survey of the Brightest Supernova Remnants in the Large Magellanic Cloud

Zachary I. Edwards  
*Columbus State University*

Follow this and additional works at: [http://csuepress.columbusstate.edu/theses\\_dissertations](http://csuepress.columbusstate.edu/theses_dissertations)



Part of the [Earth Sciences Commons](#)

---

## Recommended Citation

Edwards, Zachary I., "XMM-Newton Survey of the Brightest Supernova Remnants in the Large Magellanic Cloud" (2012). *Theses and Dissertations*. Paper 162.

This Thesis is brought to you for free and open access by CSU ePress. It has been accepted for inclusion in Theses and Dissertations by an authorized administrator of CSU ePress.

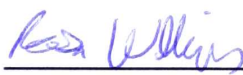



XMM-NEWTON SURVEY OF THE BRIGHTEST SUPERNOVA REMNANTS  
IN THE LARGE MAGELLANIC CLOUD

Zachary I. Edwards

**XMM-Newton Survey of the Brightest Supernova Remnants  
in the Large Magellanic Cloud**

**By  
Zachary I. Edwards**

**A Thesis Submitted in Partial Fulfillment of  
Requirements of the CSU Honors Program  
for Honors in the degree of  
Bachelor of Science  
In  
Earth and Space Science: Astrophysics & Planetary Geology  
College of Letters and Sciences  
Columbus State University**

Thesis Advisor	<u></u>	Date <u>11/26/12</u>
Committee Member	<u></u>	Date <u>11/26/12</u>
Honors Committee Member	<u></u>	Date <u>11/26/12</u>
Director, Honors Program	<u></u>	Date <u>11/26/12</u>

## 1. Introduction

Supernovae (SNe) are the primary mechanisms responsible for the enrichment of heavier elements in a galaxy. Before the event, these stars fuse heavy elements up to iron in their cores. As the star explodes the elements which have been created via fusion in the stars core are distributed to the surrounding areas. Elements heavier than iron can be formed during the explosion of the supernova. This contribution to the surrounding interstellar medium (ISM) is critical in understanding of the evolution of the galaxy and dynamics of the internal gas. As the ejecta from the supernova spreads out this left over material creates a supernova remnants (SNRs). The dust and gas components apart of the SNRs are able to provide understanding of both the galaxy and ISM. SNRs not only enrich and heat the ISM, but offers insight to the nature of the supernova (SN) which created the remnant. X-ray images and spectra give us the ability to examine the structure and evolution of hot plasma in the interior of the remnants since a majority of elements emit lines in the x-ray spectrum. Thus, the contribution from these SNRs can be understood by the abundances of their dust and gas.

There are a variety of supernovae each with distinct progenitor system and characteristics, primarily Type II and Type Ia. During a Type II (Core Collapse) Supernova lighter elements are fused into heavier elements until iron is reached in the core and no longer produces energy. After this, the star begins to swell and begins expelling its outermost layers as fusion changes throughout the star. With no outwards force provided by the heat from fusion, gravitational force causes the star to collapse. However, the force of the rebound ejects all remaining outer layers leaving behind only the star's core. During this explosion This enriches the ISM with large abundances of various elements. Therefore, the signs of a core collapse supernova is the enrichment elements such as oxygen, magnesium, silicon and neon with a depletion in iron. Type Ia supernovae involve a



Carbon-Oxygen burning White Dwarf in binary orbit with a companion star. It is accepted that the detonation is caused by a run away thermonuclear explosion of a carbon-oxygen white dwarf (WD) that has increased in mass to the Chandrasekhar limit, the mass at which the white dwarf can no longer sustain equilibrium ( $1.4M_{\odot}$ ), via mass transfer from a companion star. Since these supernovae are from evolved white dwarf stars, their respective spectrum is hydrogen poor and rich in carbon, oxygen, and iron.

The primary source of energy, hot gas, and metals in the ISM come from SNe in the form of SNRs. Stellar winds also contribute, but to a much lesser extent than SNRs. These inputs are the major regulating mechanisms of both the structure and evolution of the ISM, and in turn the host galaxy. The energy and heavy element inputs from these events influence future generations of star formation which then affect the stellar populations and subsequent rates of supernovae per galaxy. In particular, the energy input by SNe is a vital factor in the dynamical evolution of galaxies (Thornton et al. 1998). Therefore, a realistic understanding of SN contribution from SNRs populations is needed to model the evolution of a galaxy.

To quantify these effects requires the knowledge of the number, spatial distribution, progenitor types and the physical characteristics of the SNRs in the host galaxy. However, there are several difficulties which arise. During the late stages of SNR evolution there exists a complex interaction depending on the characteristics of the original SN, the shell expansion, and the surrounding ISM. Due to difficulties in detecting the faint emission from these objects the later phases in evolution have not been studied. This makes it difficult to distinguish the SNR progenitor types from the ejecta from supernova. Also, obtaining a complete census of the SNRs within a galaxy is complicated by the obscuration from the galactic plane, gaseous nebula, and other environmental factors which contribute to a high interstellar absorption in the galaxy. This interstellar absorption blocks the light provided

from these SNR and thus makes it difficult to observe.

Even though SNe and SNRs in our galaxy have been studied in-depth uncertainties in distance and high absorption from the galactic plane makes it difficult to study older, fainter objects (Green 2004). Thus, there is not an accurate account of the entire population of SNRs and their effect on the host galaxy's evolution. This can be counteracted by looking at SNRs within the Magellanic Clouds (MC) which are satellite galaxies to the Milky Way. The MC system consists of both the Large Magellanic Cloud (LMC) and the Small Magellanic Cloud (SMC). The LMC at a known distance of 50 kiloparsecs, has relatively low interstellar absorption due to its high galactic latitude. The LMC is ideal for this study since they provide a clear view of its own SNR populations.

The LMC offers the opportunity to provide insight into the above questions since it provides a near complete and un-obscured population of supernova remnants. By studying the SNR development with a examination of the properties of the MC SNRs, contributions of SNR to their host galaxy will be able to be quantified and later used as a rough comparison for other galaxies. For preliminary results, analysis of the population of SNR as well as their contributions of diffuse materials within the LMC will be studied. The contribution provided from other diffuse materials, such as Super Bubbles, in the LMC and SMC will be left for another study.

This survey of SNR contribution to the LMC can be conducted with the advantages presented with both the LMC and x-ray coverage from the XMM-Newton satellite. Using the x-ray spectrum, models of thermal plasma including thermal Bremsstrahlung and line emission will allow for analysis of elemental contribution. Thus, estimates of various physical properties for the x-ray emitting plasma such as the density of the hot gas are able to be calculated. Free parameters in these spectral fits will contribute to the understanding of emission lines from the x-ray spectrum. Most notable are the Fe bands which give insight

into the iron abundance of a given source making Type Ia SNRs distinguishable from Type II remnants (e.g., Hughes et al. 2003; Hendrick et al. 2003; Borkowski et al. 2003; Hughes et al. 1995). This allows for a statistical examination of SNRs within the LMC via x-ray spectral analysis.

An underlining goal of this survey is to better catalog these SNRs. Currently a comprehensive database ([www.mcsnr.org](http://www.mcsnr.org)) exists and already provides some data and information. Multi-wavelength images, consisting of radio, optical, x-ray, and infrared wavelengths, will be constructed for use with this database. For the scope of this database, as well as the above mentioned survey, a SNR will be defined as a diffuse object that meets two of the three following requirements: 1) Diffuse non-thermal radio emission, 2) diffuse thermal X-ray emission, and 3) High optical  $[SII]/H\alpha$  ratio ( $>0.4$ ) and/or high optical expansion velocity. Table 1 lists confirmed SNR within the LMC to be studied during this analysis with priority given to the brightest SNR. The Primary products are provided from the XMM-Newton x-ray observatory public data archive and have gone through standard processing steps to allow the data to be calibrated. Several ground-based projects will be used to supplement the space telescope data including the Australia Telescope Compact Array (ATCA) survey of the entire LMC in the radio spectrum. Cerro Tololo data will be used to provided the optical counterpart from the Magellanic Clouds Emission-Line Survey (MCELS). Infrared data provided by the Spitzer Space Telescope will be used in place of optical for remnants that lack coverage or have faint emission from optical counterparts.



SNR Name	RA (J2000)	DEC (J2000)	Flux (ergs/cm <sup>2</sup> /s)
MCELS J0448-6658	04:48:22	-66:59:52	???
MCELS J0449-6921	04:49:20	-69:20:20	$<4.0 \times 10^{-12}$
0450-709	04:49:20	-70:50:20	$2.4 \times 10^{-13}$
LHa 120-N4D	04:53:10	-66:54:40	$3.0 \times 10^{-13}$
0453-685	04:53:35	-68:29:40	$1.7 \times 10^{-11}$
LHa 120-N9	04:54:35	-67:12:40	$1.3 \times 10^{-12}$
LHa 120-N11L	04:54:50	-66:25:35	$3.0 \times 10^{-13}$
LHa 120-N86	04:55:45	-68:39:05	$8.0 \times 10^{-13}$
LHa 120-N186D	04:59:50	-70:07:50	$9.9 \times 10^{-13}$
DEM L71	05:05:45	-67:53:00	$2.4 \times 10^{-11}$
LHa 120-N23	05:05:52	-68:01:40	$7.4 \times 10^{-11}$
MCELS J0506-6541	05:06:05	-65:41:08	$1.1 \times 10^{-12}$
0509-687	05:09:00	-68:43:30	$4.7 \times 10^{-11}$
0509-675	05:09:32	-67:31:30	$4.7 \times 10^{-11}$
DEM L109	05:13:12	-69:12:20	???
LHa 120-N120	05:18:45	-69:39:10	$3.0 \times 10^{-13}$
0519-690	05:19:36	-69:02:10	$3.4 \times 10^{-11}$
0520-694	05:19:45	-69:26:00	$1.0 \times 10^{-12}$
MCELS J0521-6542	05:21:39	-65:43:07	???
LHa 120-N44	05:23:12	-67:52:40	$5.0 \times 10^{-13}$
DEM L175a	05:24:40	-66:25:00	???
LHa 120-N132D	05:25:03	-69:38:30	$3.0 \times 10^{-10}$
0525-660	05:25:28	-65:59:15	$6.4 \times 10^{-11}$
LHa 120-N49	05:25:59	-65:05:00	$6.3 \times 10^{-11}$
0528-692	05:27:35	-69:12:10	$3.0 \times 10^{-13}$
DEM L204	05:27:55	-65:49:40	$4.0 \times 10^{-13}$
HP99 498	05:28:20	-67:13:40	$6.0 \times 10^{-13}$
DEM L214	05:29:50	-66:53:50	???
DEM L218	05:30:40	-70:07:30	???
LHa 120-N206	05:31:55	-71:00:30	$4.0 \times 10^{-12}$
0532-675	05:32:20	-67:31:40	$4.0 \times 10^{-13}$
0534-699	05:34:00	-69:55:20	$2.5 \times 10^{-11}$
DEM L238	05:34:10	-70:33:45	$6.7 \times 10^{-13}$
SN 1987A	05:35:27	-69:16:10	$1.0 \times 10^{-12}$
LHa 120-N63A	05:35:44	-66:02:10	$2.2 \times 10^{-10}$
Honeycomb	05:35:45	-69:18:05	$5.6 \times 10^{-13}$
LHa 120-N59B	05:36:05	-67:35:30	???
0540-697	05:40:00	-69:45:10	$2.4 \times 10^{-12}$
0540-693	05:40:09	-69:19:50	$1.1 \times 10^{-11}$
DEM L299	05:43:20	-68:58:40	$8.0 \times 10^{-12}$
DEM L316B	05:47:00	-69:42:40	$1.5 \times 10^{-12}$
DEM L316A	05:47:20	-69:41:30	$9.7 \times 10^{-13}$
0548-704	05:47:50	-70:24:50	$2.4 \times 10^{-11}$
J0550-683	05:50:30	-68:22:40	$5.4 \times 10^{-12}$

Table 1: Confirmed SNR within the LMC with given X-ray Flux (Williams 1999; Seward 2012; Klimek 2009). It will be assumed that each SNR is at the same distance away as the



## 2. Observations

Space observatories have to be used for analysis x-ray data due to the atmosphere being opaque to x-rays. A complete survey of LMC SNRs can now be done due to advances in x-ray observations as presented by satellites such as XMM-Newton. A complete survey of the LMC SNRs is in progress and to be completed by XMM-Newton and individual SNRs have been studied with Chandra. Both satellites present their own advantages with Chandra having high spatial resolution and XMM-Newton being more sensitive to x-rays. In order for an in-depth study of the diffuse material of these SNRs the higher x-ray sensitivity provided by XMM-Newton offers the better capability as opposed to Chandra.

The European Space Agency's X-ray Multi-Mirror Mission was launched in 1999 and has since been observing various high energy phenomena across the sky. To capture data XMM-Newton has three sets of CCD (Charged Coupled Devices). The Metal Oxide Semi-conductor (MOS) cameras consist of seven front-illuminated CCDs which allows for high energy photons to be observed. The effective energy range of this instrument is 0.2-10keV.

XMM-Newton archival data was used for this study. Table 2 presents the 10 brightest ( $>10 \times 10^{-11}$  ergs/cm<sup>2</sup>/s) SNRs with current coverage and available public data. These 10 SNR provide an excellent sample of the total 43 confirmed SNRs in the LMC since it includes the four known Type Ia Supernovae as well as six of the youngest Type II SNe in the LMC. This allows preliminary information and patterns to be distinguished from these young SNRs. This sample excludes the older and more diffuse remnants which are required for a complete survey, however; the material from these older SNRs in most cases would be indistinguishable from the ISM and therefore be harder to study.

SNR Name	RA (J2000)	DEC (J2000)	Progenitor Type
0453-685	04:53:35	-68:29:40	Core Collapse
DEM L71	05:05:45	-67:53:00	Type Ia
LHa 120-N23	05:05:52	-68:01:40	Core Collapse
0509-687	05:09:00	-68:43:30	Type Ia
0509-675	05:09:32	-67:31:30	Type Ia
0519-690	05:19:36	-69:02:10	Type Ia
LHa 120-N132D	05:25:03	-69:38:30	Core Collapse
0525-660	05:25:28	-65:59:15	Core Collapse
LHa 120-N49	05:25:59	-65:05:00	Core Collapse
LHa 120-N63A	05:35:44	-66:02:10	Core Collapse

Table 2: Brightest SNRs within the LMC and their known type. The above 4 Type Ia SNRs are known to be Type Ia from analysis of their Light Echoes (Rest et al. 2005; 2008) + Hydrogen Balmer Lines

Figures 1-10 shows the XMM-Newton observation of each individual SNR. Each image was taken using the EMOS1 instrument of XMM-Newton and spans across the entire effective sensitivity range of the instrument, approximately 0.2-10 keV. These images were reduced using standard procedures in the Science Analysis Software (SAS) data reduction package. Each of the SNR's emission was best fitted to either an ellipse or circle depending on its geometry of the x-ray emitting gas. This is required in order to calculate volume and density of the hot plasma. Also, the centers of these fits will be used to provide a location, of the x-ray emission of the SNR, for the MCSNR database.

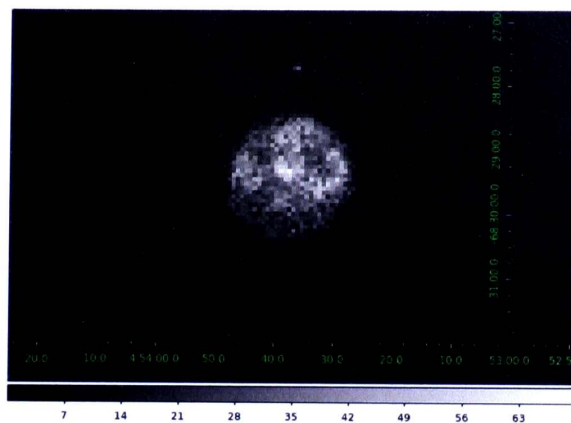


Fig. 1.— SNR 0453-68.5 is best fitted by a circle with a measured radius of 67.11 Arcseconds ( $5.02 \times 10^{19}$  cm).

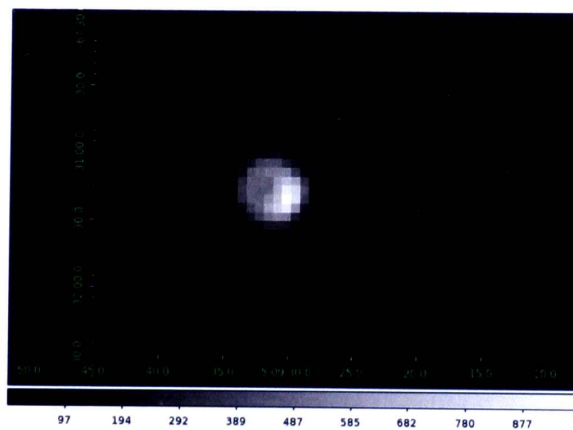


Fig. 2.— SNR 0509-67.5 is best fitted by a circle with a measured radius of 25.12 Arcseconds ( $1.88 \times 10^{19}$  cm).



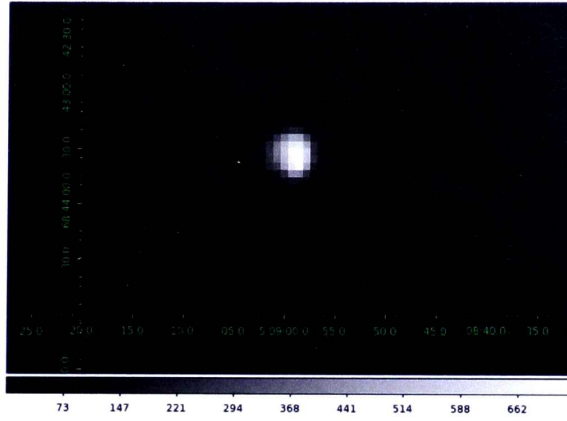


Fig. 3.— SNR 0509-68.7 is best fitted by a circle with a measured radius of 24.15 Arcseconds ( $1.81 \times 10^{19}$  cm).

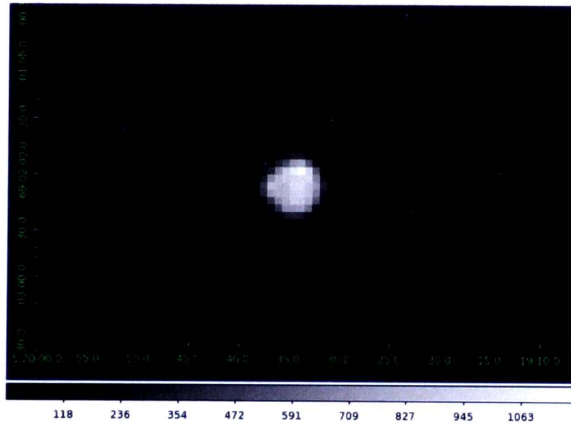


Fig. 4.— SNR 0519-69.0 is best fitted by a circle with a measured radius of 20.36 Arcseconds ( $1.52 \times 10^{19}$  cm).

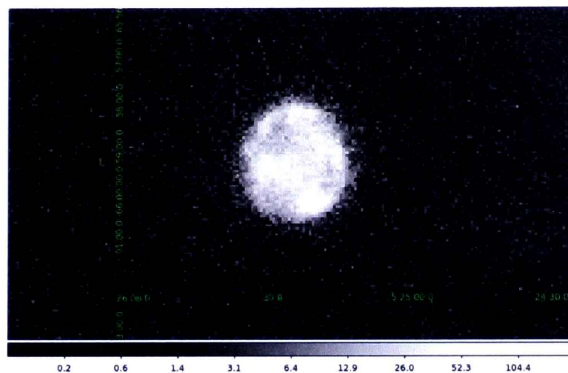


Fig. 5.— SNR 0525-66.0 is best fitted by a circle with a measured radius of 82.29 Arcseconds ( $6.16 \times 10^{19}$  cm).

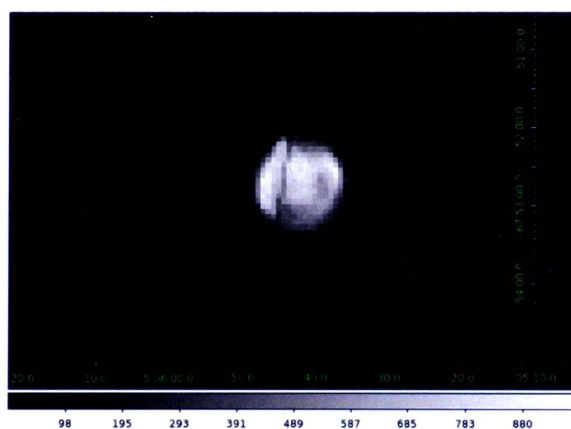


Fig. 6.— SNR DEM L71 is best fitted by a circle with a measured radius of 41.04 Arcseconds ( $3.07 \times 10^{19}$  cm).

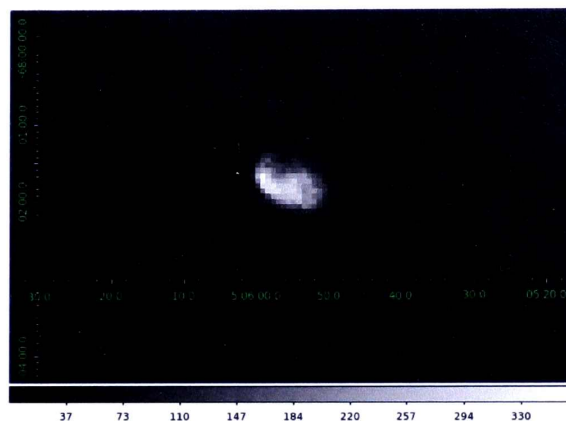


Fig. 7.— SNR LHa 120-N23 is best fitted by a circle with a measured radius of 36.90 Arcseconds ( $2.76 \times 10^{19}$  cm).

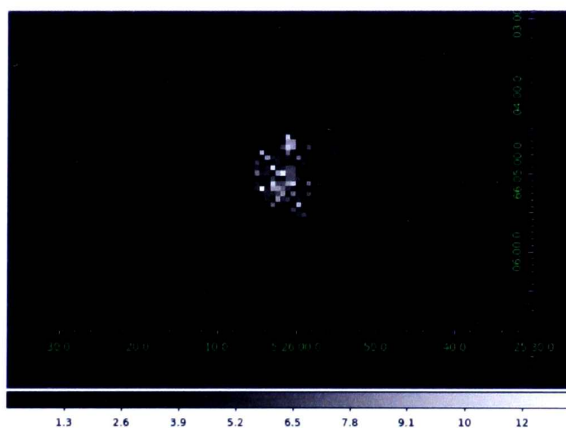


Fig. 8.— SNR LHa 120-N49 is best fitted by a circle with a measured radius of 82.29 Arcseconds ( $6.12 \times 10^{19}$  cm).



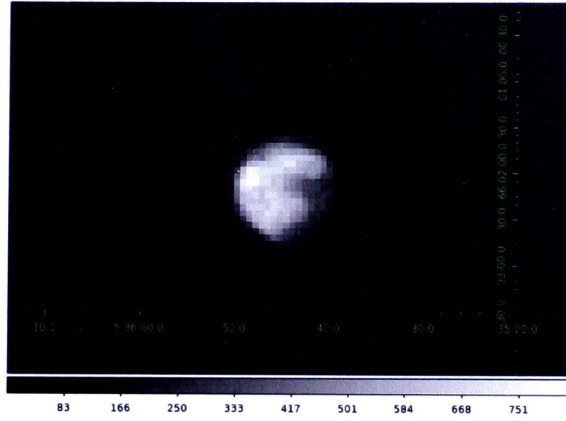


Fig. 9.— SNR LHa 120-N63A is best fitted by a circle with a measured radius of 39.46 Arcseconds ( $2.95 \times 10^{19}$  cm).

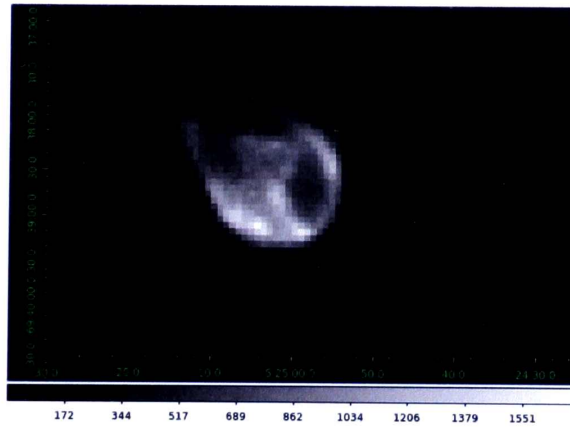


Fig. 10.— SNR LHa 120-N132D is best estimated by an ellipse with a semi-major axis of 72.72 Arcseconds and semi-minor axis of 52.50 Arcseconds ( $5.44 \times 10^{19}$  cm &  $4.08 \times 10^{19}$  cm respectively).

### 3. Data Analysis

Fitting models to the spectral observations is required in order to infer abundance of various elements. Since SNRs in this sample are young, the initial shock from the explosion is still causing ionization to occur. Also, even though the Magellanic Cloud is largely un-obscured by interstellar dust, there is still a small amount of absorption between the LMC and the Milky Way galaxy. Therefore, the model has to be representative of these conditions. To account for these physical situations a multiplicative model of `vnshock` combined with `wabs` is used to fit the observations for XMM-Newton.

The `vnshock` component is a plane-parallel shock plasma model which accounts for separate ion and electron temperatures as well as emission lines from Carbon, Nitrogen, Oxygen, Neon, Magnesium, Silicon, Sulfur, Argon, Calcium, Iron, and Nickel (Borkowski et al 2001). This provides information which accounts for emissions from the shocked material. To account for absorption of these elements from gas and dust in the line of sight, `wabs`, a photo-electric absorption is used to account for the equivalent hydrogen column using the Wisconsin cross-sections (Morrison & McCammon 1983).

For the following fits to the observed spectrum the emission lines were left as free parameters using a chi-squared statistical method. However, if the fits tended towards unrealistic values they were fixed at the average abundance of  $0.3M_{\odot}$  for the LMC (Russel & Dopita 1992). Both Hydrogen and Helium were left fixed at the cosmic value as well as nickel fixed at 30% of solar abundances. Carbon, Nitrogen, and Argon were fixed at 30% of solar abundances since their contribution to these fits were negligible and did not affect the model.

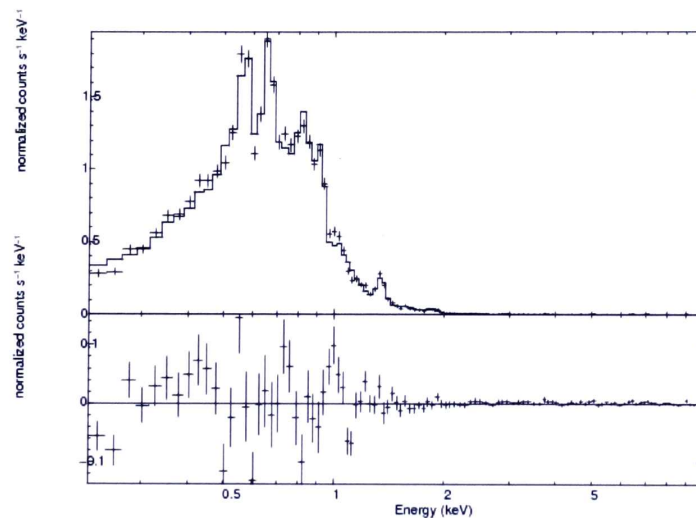


Fig. 11.— vnpshock\*wabs model fit to SNR 0453-68.5: reduced  $\chi^2 = 1.6$  for 100 degrees of freedom.

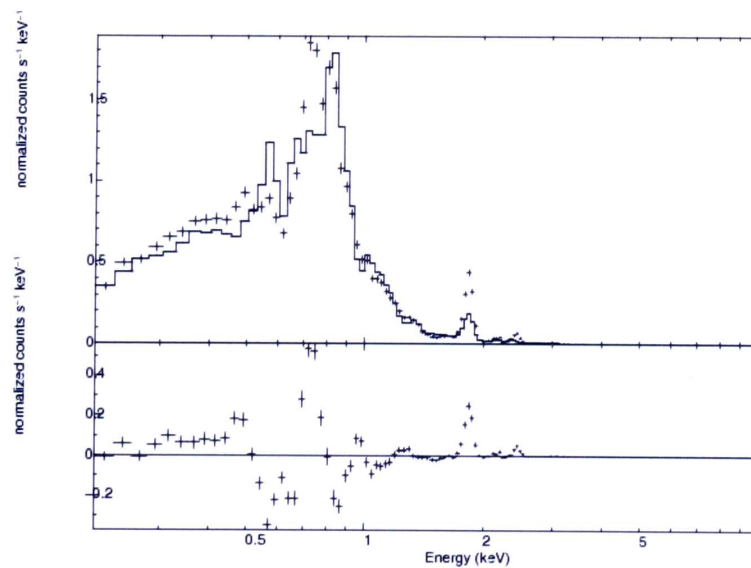


Fig. 12.— vnpshock\*wabs model fit to SNR 0509-67.5: Reduced  $\chi^2 = 23.5$  for 72 degrees of freedom.



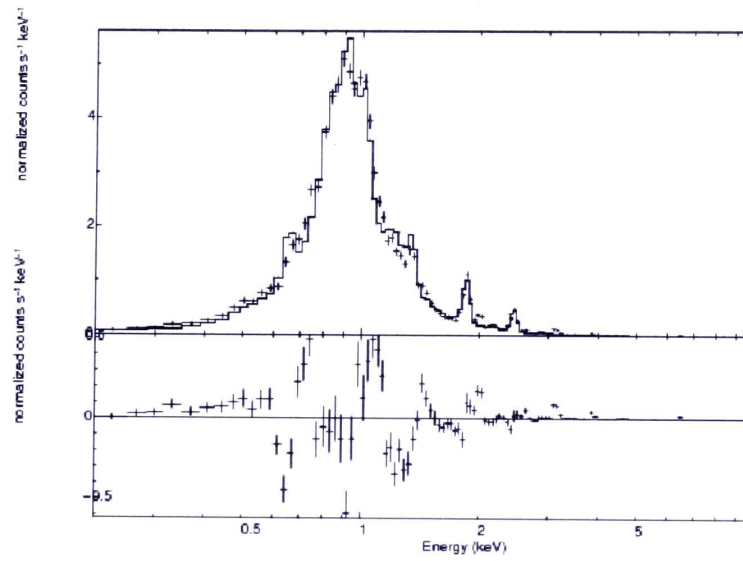


Fig. 13.— vnpshock\*wabs model fit to SNR 0509-68.7: Reduced  $\chi^2 = 8.1$  for 77 degrees of freedom.

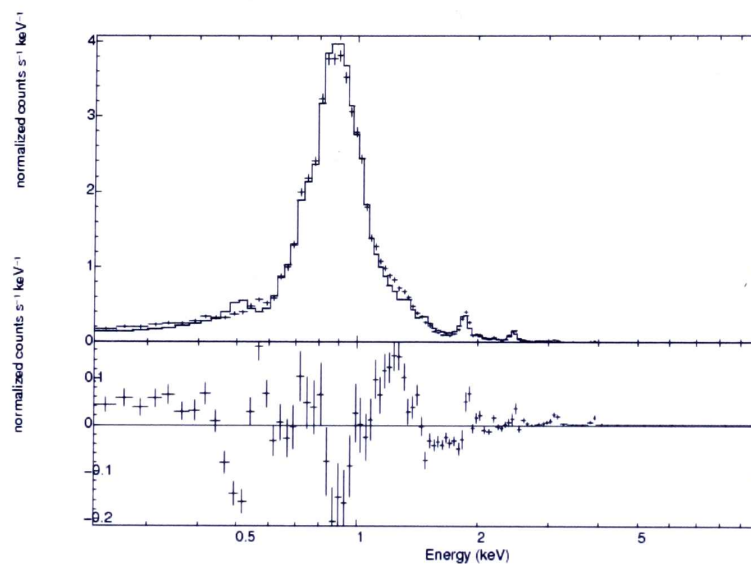


Fig. 14.— vnpshock\*wabs model fit to SNR 0519-69.0: Reduced  $\chi^2 = 7.4$  for 78 degrees of freedom.

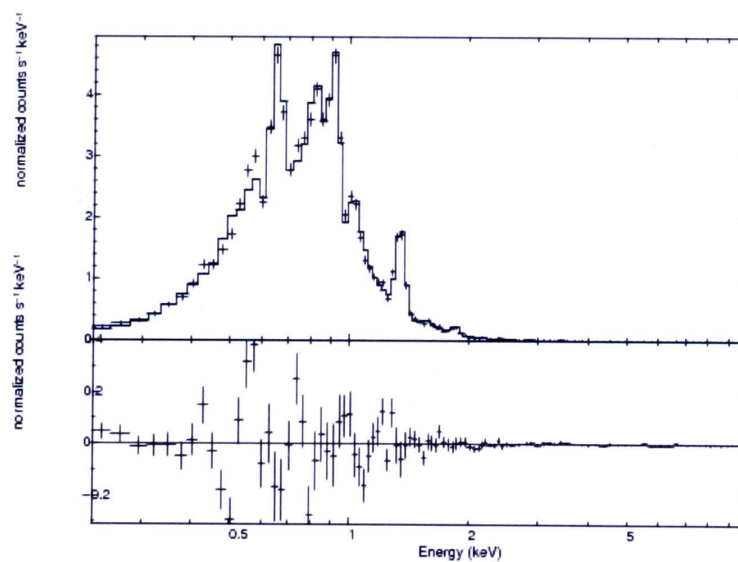


Fig. 15.— vnpshock\*wabs model fit to SNR 0525-66.0: Reduced  $\chi^2 = 1.7$  for 89 degrees of freedom.

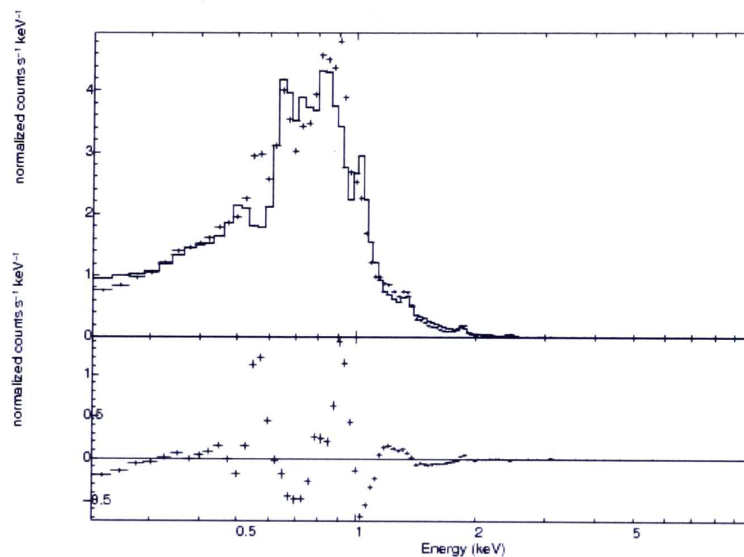


Fig. 16.— vnpshock\*wabs model fit to SNR DEM L71: Reduced  $\chi^2 = 4.9$  for 82 degrees of freedom.

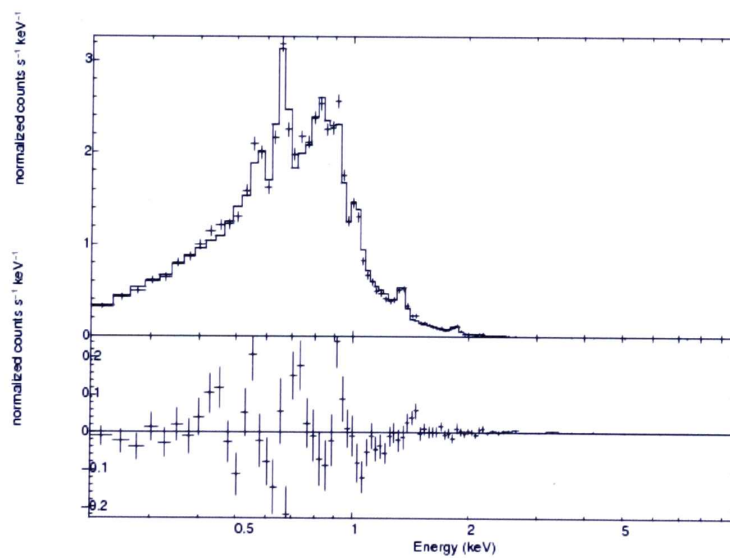


Fig. 17.— vnpshock\*wabs model fit to SNR LHa 120-N23: Reduced  $\chi^2 = 2.2$  for 67 degrees of freedom.



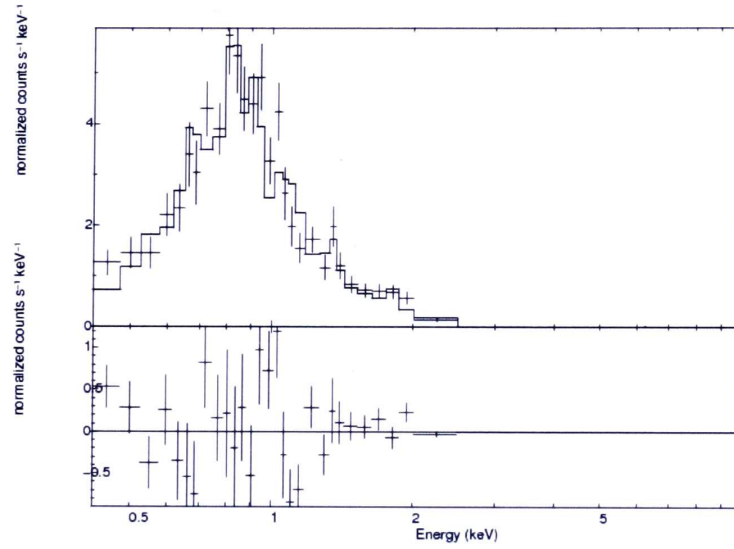


Fig. 18.— vnpshock\*wabs model fit to SNR LHa 120-N49: Reduced  $\chi^2 = 2.1$  for 21 degrees of freedom.

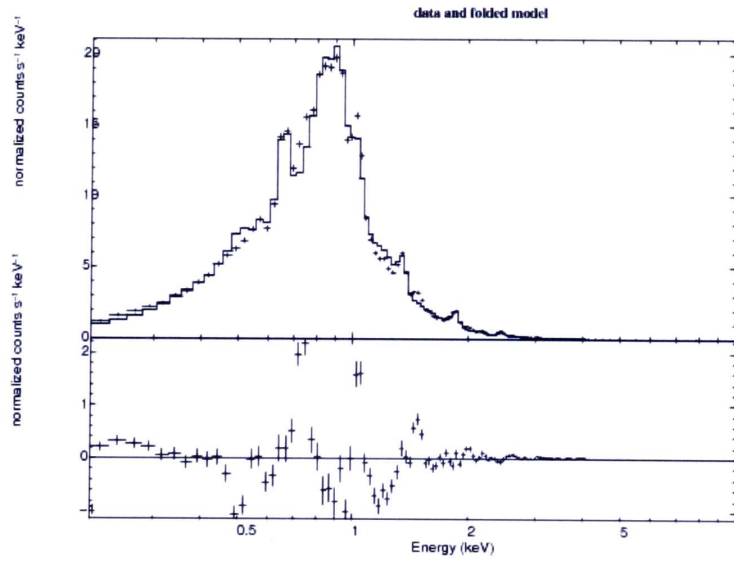


Fig. 19.— vnpshock\*wabs model fit to SNR LHa 120-N63A: Reduced  $\chi^2 = 10.7$  for 92 degrees of freedom.

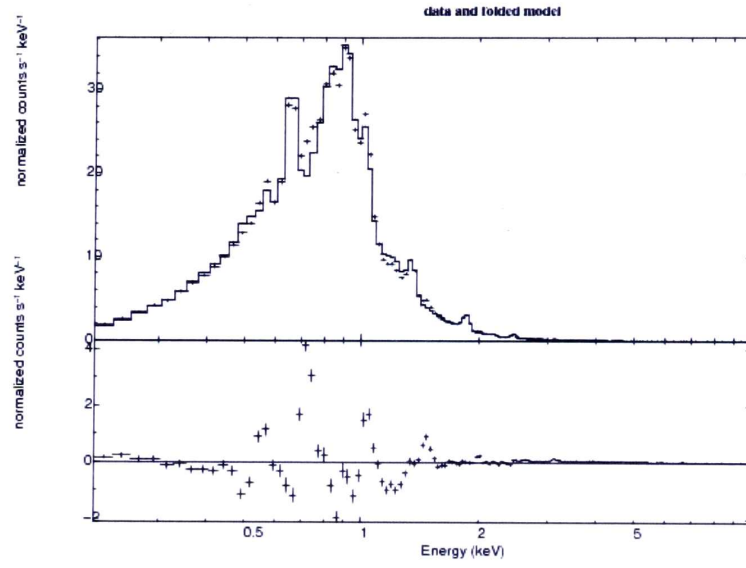


Fig. 20.— vnpshock\*wabs model fit to SNR LHa 120-N132D: Reduced  $\chi^2 = 23.8$  for 117 degrees of freedom.

SNR Name	kT <sub>a</sub>	kT <sub>b</sub>	H	He	C	N	O	Ne	Mg	Si	S	Ar	Ca	Fe	Ni
0453-685	0.755	0.022	1.000	1.000	0.300	0.300	0.194	0.235	0.323	0.246	0.300	0.300	0.300	0.224	0.300
N23	0.600	0.012	1.000	1.000	0.300	0.300	0.300	0.300	0.278	0.290	0.455	0.300	0.300	0.196	0.300
N49	0.775	0.776	1.000	1.000	0.300	0.300	0.300	0.300	0.278	0.584	0.300	0.300	0.300	0.425	0.300
0525-660	0.542	0.016	1.000	1.000	0.300	0.300	0.226	0.315	0.540	0.264	0.499	0.300	0.300	0.165	0.300
N132D	0.748	0.080	1.000	1.000	0.300	0.300	0.223	0.226	0.163	0.242	0.530	0.300	0.300	0.162	0.300
N63A	0.749	0.168	1.000	1.000	0.300	0.300	0.158	0.162	0.130	0.229	0.594	0.300	0.300	0.152	0.300
0519-690	0.722	0.034	1.000	1.000	0.300	0.300	0.300	0.300	0.193	0.924	2.389	0.300	0.300	0.709	0.300
0509-675	1.157	1.065	1.000	1.000	0.300	0.300	0.177	0.177	0.177	2.389	2.389	0.300	0.300	0.666	0.300
0509-687	0.886	0.014	1.000	1.000	0.300	0.300	0.300	0.300	0.177	0.481	1.599	0.300	0.300	0.333	0.300
DEM L71	0.770	0.087	1.000	1.000	0.300	0.300	0.294	0.428	0.351	0.407	0.595	0.300	0.995	0.425	0.300

Table 3: Abundances from best fit of vnpshock and wabs model of the brightest SNRs within the LMC. Units are in percentages of abundances of each element compared to solar abundances

SNR Name	$\tau_u$	Norm	nH	Flux	Volume	Density	Ionization Age
0453-685	$8.36 \times 10^{10}$	0.006	$0.107 \times 10^{22}$	$5.77 \times 10^{-12}$	$5.30 \times 10^{59}$	0.63	4220
N23	$4.46 \times 10^{11}$	0.011	$0.068 \times 10^{22}$	$1.01 \times 10^{-11}$	$8.81 \times 10^{58}$	2.09	6770
N49	$1.69 \times 10^{10}$	0.057	$0.468 \times 10^{22}$	$2.23 \times 10^{-11}$	$1.67 \times 10^{59}$	3.51	150
0525-660	$1.90 \times 10^{11}$	0.036	$0.257 \times 10^{22}$	$1.41 \times 10^{-11}$	$9.77 \times 10^{59}$	1.16	5190
N132D	$3.99 \times 10^{11}$	0.194	$0.140 \times 10^{22}$	$1.22 \times 10^{-10}$	$3.79 \times 10^{59}$	4.30	3000
N63A	$3.43 \times 10^{11}$	0.150	$0.180 \times 10^{22}$	$7.33 \times 10^{-11}$	$1.08 \times 10^{59}$	7.08	1500
0519-690	$9.49 \times 10^{11}$	0.012	$0.154 \times 10^{22}$	$1.35 \times 10^{-11}$	$1.48 \times 10^{58}$	5.33	5600
0509-675	$2.23 \times 10^{10}$	0.002	$0.080 \times 10^{22}$	$6.38 \times 10^{-12}$	$2.78 \times 10^{58}$	1.65	430
0509-687	$3.21 \times 10^{11}$	0.055	$0.406 \times 10^{22}$	$2.11 \times 10^{-11}$	$2.47 \times 10^{58}$	8.94	1100
DEM L71	$2.71 \times 10^{11}$	0.009	$0.046 \times 10^{22}$	$1.64 \times 10^{-11}$	$1.21 \times 10^{59}$	1.67	5200
Units	s*Particle/cm <sup>3</sup>		cm <sup>2</sup>	ergs/cm <sup>2</sup> /s	cm <sup>3</sup>	Particle/cm <sup>3</sup>	Years

Table 4: Calculated values from fit of vnpshock and wabs model of SNRs within the LMC. Also, the measured flux from these observations are presented. Note that a few of them vary from the flux chosen in Table 1. Also, Normalization (Norm) is in units of a complex function of density.

The free parameters in these spectral fits to the emission lines include abundances of the various elements, in units of solar abundances, that are major contributors of lines in the x-ray spectrum. Most notable are the iron lines which provides information into the amount of iron in the given source. From the abundance of iron, it is possible to infer the progenitor type of SN since it is expected for all iron in a core collapse SN to be in the left over core whereas a Type Ia would expel any iron.

The normalization parameter from this thermal plasma model is related x-ray emissivity of the plasma and therefore able to provide information on the density of the hot gas if the volume of the gas is known as given by  $n_H = 3.89 \times 10^7 \sqrt{(\frac{Z^2 \eta}{V})}$ . Where  $Z$  is the



distance in centimeters,  $\eta$  is the normalization obtained from the fitted data, and  $V$  is the volume of the hot plasma. Within the plane-parallel thermal plasma shock model, there is a  $\tau$  parameter which indicates the ionization timescale. This parameter consists of density multiplied by the time to reach the current ionization state. From the  $\tau$  parameter, the ionization can be calculated which measures the time it has taken to reach the current state of non-equilibrium. Note that the actual ages, measured from expansion velocities, can be measured to be higher and that this calculation only places a lower limit on the age of the SNR.

#### 4. Summary

It can be seen from Table 3 that the four Type Ia SNRs are enriched with iron where as the Type II SNRs are slightly depleted due to the majority of iron being caught up in the leftover core of the massive star. Therefore the population of Type Ia SNe are responsible for the enrichment and primary contribution of iron into the surrounding ISM. However, the Type II SNRs are slightly more enriched in oxygen, silicon, sulfur, and magnesium.

Also, an expected trend can be seen between the ionization age and size of the SNRs. The smaller SNRs such as SNR 0509-67.5, 0509-68.7, and N63A are relatively young,  $<1,500$  years. Whereas larger remnants such as 0525-66.0, N132D, and 0453-68.5 are much older,  $\geq 3,000$  years. This is due to the fact that older SNRs have more time to expand to there current state. However N49, 0519-69.0, and N23 do not follow this trend which is most likely due to interactions with higher density areas in the surrounding dust and gas in the ISM.

From these SNRs it can be seen that there is an obvious enrichment in metals such as oxygen, silicon, sulfur, and magnesium. The primary contribution of iron is provided by the

four Type Ia SNRs. Also, the fits of the Type Ia tended towards 1-3 times solar abundances which is possible due to the young physical ages of these SNR as well as their detonation mechanisms. This enrichment of gas provided from these SNRs thus contribute to the overall abundance in the interstellar medium which in turn affects the chemical evolution of the host galaxy. In order to get a complete picture of dust contribution, the remaining 33 SNRs will need to be analyzed and add to this study. Also, other diffuse materials primarily from superbubbles, will also need to be analyzed in the x-ray spectrum.

I would like to acknowledge Dr. Rosa N. Williams for agreeing to be the advisor & mentor for this study as well as Dr. Shawn Cruzen & Dr. Troy Vidal being apart of the Honors Thesis Committee. Also, I would like to thank Dr. Cindy Ticknor and the Honors Program for their continued support in this research and my academic endeavors.

## REFERENCES

- Chu, Y.-H. 1997, AJ, 113, 1815
- Chu, Y.-H. & Kennicutt, R. C. Jr. 1988a, AJ, 95, 1111
- Chu, Y.-H. & Kennicutt, R. C. Jr. 1988b, AJ, 96, 1874
- Cooper, R. L., Guerrero, M. A., Chu, Y.-H., Chen, C.-H., & Dunne, B. C. 2004, ApJ, 605, 751
- Borkowski et al., 2001, ApJ, 548, 820
- Dickel, J. R., McIntyre, V., Gruendl, R. A., & Milne, D. K. 2004, AJ, to be submitted
- Dickel, J. R., Williams, R. M., Carter, L. M., Milne, D. K., Petre, R., & Amy, S. W. 2001, AJ, 122, 849
- Dunne, B. C., Points, S. D., & Chu, Y.-H. 2001, ApJS, 136, 119
- Feast, M. 1999, IAUS, 190, 542
- Green, D. A. 2004, 'A Catalogue of Galactic Supernova Remnants (2004 January Version)', Mullard Radio Astronomy Observatory, Cavendish Laboratory, Cambridge, UK
- Hendrick, S. P., Borkowski, K. J., & Reynolds, S. P. 2003, ApJ, 593, 370
- Hughes, J. P., Hayashi, I., & Koyama, K. 1998, ApJ, 505, 732
- Hughes, J. P., Ghavamian, P., Rakowski, C. E., & Slane, P. O. 2003, ApJL, 582, 95
- Klimek et al. 2010, ApJ, 725, 2281
- Mac Low, M.-M., McCray, R. A., & Norman, M. L. 1989, ApJ, 337, 141

- Mathewson, D. S., Ford, V. L., Dopita, M. A., Tuohy, I. R., Long, K. S. & Helfand, D. J. 1983, *ApJS*, 51, 345
- McKee, C. F. & Ostriker, J. P. 1977, *ApJ*, 218, 148
- Morrison & McCammon 1983 *ApJ* 270, 119
- Park, S. et al. 2003, *ApJL*, 598, 95
- Rest, A. et al. 2005, *Nature*, 438, 1132
- Rest, A. et al. 2008, *ApJ*, 680, 1137
- Reynolds, S. P. 1998, *ApJ* 493, 357
- Russel & Dopita 1992, *ApJ*, 384, 508
- Shelton, R. 1999, *Apj*, 521, 217
- Slavin, J. D., & Cox, D. P. 1992, *ApJ*, 392, 131
- Slavin, J. D., & Cox, D. P. 1993, *ApJ*, 417, 187
- Seward, F. D., et al. Chandra SNR Catalog, <http://hea-www.harvard.edu/ChandraSNR/>
- Thornton, K., Gaudlitz, M., Janka, H.-Th., & Steinmetz, M. 1998, *ApJ*, 500, 95
- Williams, R. N. M. et al. 1999, *ApJ*, 514, 798
- Williams, R. M., Chu, Y.-H., Dickel, J. R., Petre, R., Smith, R. C., & Tavaréz, M. 1999, *ApJS*, 123, 467
- Williams, R. M., Chu, Y.-H., Dickel, J. R., Gruendl, R. A., Shelton, R., Points, S. D. & Smith, R. C. 2004, *ApJ*, 613, 948



Williams, R. M., Chu, Y.-H., Dickel, J.R., Grundl, R. A., Gurrero, M. A., Seward, F. D., &  
Hobbs, G. 2005, ApJ, 638, 704

Williams, R. M., Chu, Y.-H., Dickel, J. R., Et al 1999, ApJS, 123, 467 maybe